Refractive index tomography of myelinating glial cells

Toy, Muhammed Fatih, Vatandaslar, Burcu Kurt, Kerman, Bilal Ersen

Muhammed Fatih Toy, Burcu Kurt Vatandaslar, Bilal Ersen Kerman, "Refractive index tomography of myelinating glial cells ," Proc. SPIE 10887, Quantitative Phase Imaging V, 1088713 (4 March 2019); doi: 10.1117/12.2512706

SPIE.

Event: SPIE BiOS, 2019, San Francisco, California, United States

Refractive index tomography of myelinating glial cells

Muhammed Fatih Toy*[a], Burcu Kurt Vatandaşlar[b], Bilal Ersen Kerman[b]
[a] School of Engineering and Natural Sciences, Istanbul Medipol University, Turkey
[b] Research Center for Regenerative and Restorative Medicine (REMER), Istanbul Medipol University, Turkey

ABSTRACT

Refractive index tomography as an emerging technique enables the 3D morphological investigation of cells with no marker. Here, refractive index tomographic imaging of myelinating glial cells is presented. Myelin as a signal insulation layer around an axon is formed by the wrapping of Schwann cells or oligodendrocytes. Microscopic investigation of myelination traditionally requires fluorescent markers. Glial cells generally wrap the axon for more than ten layers. This multilayer formation has alternating and uniform layers of protein and lipid. Earlier studies on the structure of the myelin sheath have shown that the thickness period is lower than 20nm including the thickness of the extracellular medium after each layer. Direct observation of an individual layer is not possible (using classical microscopy techniques) due to dimensions being very small compared to the wavelength of the illumination light. However, periodic nature of the layers enables the differentiation of a myelinated axon from an unmyelinated one. Rapid change of the integrated refractive index and the Bragg fiber like structure alters the transmission behavior as a function of wavelength and incidence angle. With the 3D sectioning capability of refractive index tomography, these features can be easily identified.

Keywords: Refractive index tomography, quantitative phase tomography, myelin

1. INTRODUCTION

Quantitative phase microscopy has gained interest as a label free approach of evaluating morphological and chemical parameters of live cell samples. Quantitative perspective of the approach as the phase signal reflects the variations in the axially integrated optical path length. This path length includes both the morphology and the refractive index variations. Eventually, unambiguous assessment of refractive index distribution in a volume requires extension of the technique with tomographic imaging capability. In transmitted light scheme, angular scanning of the illumination beam and sample rotation are the two most common approaches to harvest axial information [1, 2].

In the central nervous system (CNS) the speed of signal transmission along the axons are increased by myelination [3]. Cellular membranes of oligodendrocytes, which are a subtype of the glial cells, insulate the axons by forming layers cholesterol-rich membrane that wraps the axon, the myelin. Myelin is not only essential for efficiency and plasticity of the brain's computational process but also supports survival of neurons [3]. Therefore, myelin is indispensable for proper brain function and any damage to myelin such as in multiple sclerosis MS, disrupts CNS function [4]. Labeled imaging of the myelin cannot benefit from the fluorescence selectivity due to the unavailability to a specific marker. Membrane markers that label the entirety of the cell membrane are generally utilized. Significant increase of the signal is typically interpreted as the formation of the myelin. On the label free imaging front, periodic structure of the myelin with a period of approximately 20nm [5] is not possible image directly. Interestingly the radial symmetry and the contrasting refractive index of the individual layers brings resemblance to Bragg fibers. Respectively, the Fresnel law may be utilized to analyze spectral amplitude signal modulation in the myelin region. This signal modulation was used for the label free direct imaging of the myelin Alternative, nonlinear imaging was utilized to benefit from the periodic structure [6]. Here, the effective refractive index change due to the angular variation of the incident light is benefited from to be able discern the myelinated axons from the unmyelinated ones.

Quantitative Phase Imaging V, edited by Gabriel Popescu, YongKeun Park, Proc. of SPIE Vol. 10887, 1088713

2. MATERIALS AND METHODS

2.1 Oligodendrocyte & Neuron Co-Culturing

The myelin was analyzed in in vitro co-cultures of neurons and oligodendrocytes established as was described previously [7]. Briefly, oligodendrocytes and neurons were generated from neural progenitor cells (NPCS) derived from mouse embryonic stem cells (mESCs). For oligodendrocyte differentiation, NPCs were grown in DMEM/F12 medium supplemented with N2, B27 and first insulin-like growth factor 1 and platelet-derived growth factor-alpha and next ciliary neurotrophic factor, neurotrophin-3 and triiodothyronine (T3). For neuronal differentiation, NPCs were grown in DMEM/F12 medium supplemented with N2, B27, glial cell derived neurotrophic factor, cyclic AMP and ascorbic acid. Co-cultures were maintained in neuronal medium with the addition of T3 [7].

2.2 Refractive Index Tomography Setup

The experimental setup is based on a Mach-Zehnder type interferometer as illustrated in figure 1 in which the collimated illumination from a laser source at 520nm is split in two arms by a polarizing beam splitter. On one arm, the collimated beam is expanded and its convergence is controlled by an additional lens. On the other arm, a motorized mirror angularly scans the beam direction in a cone of maximal 4 degrees. The scanned beam is enlarged using a telescope assembly. Enlarged beam is incident to a microscopy tube lens and a 20X 0.5NA microscope objective sequentially. At the working plane of this objective the sample is positioned. The sample is imaged to a CCD camera through another microscope objective with NA of 0.5, magnification of 20X and a matching microscopy tube lens. A beam splitter positioned just before the camera recombines the arms of the interferometer. The angular orientation of this beam splitter is adjusted to provide off-axis holograms on the camera plane with optimal sampling.

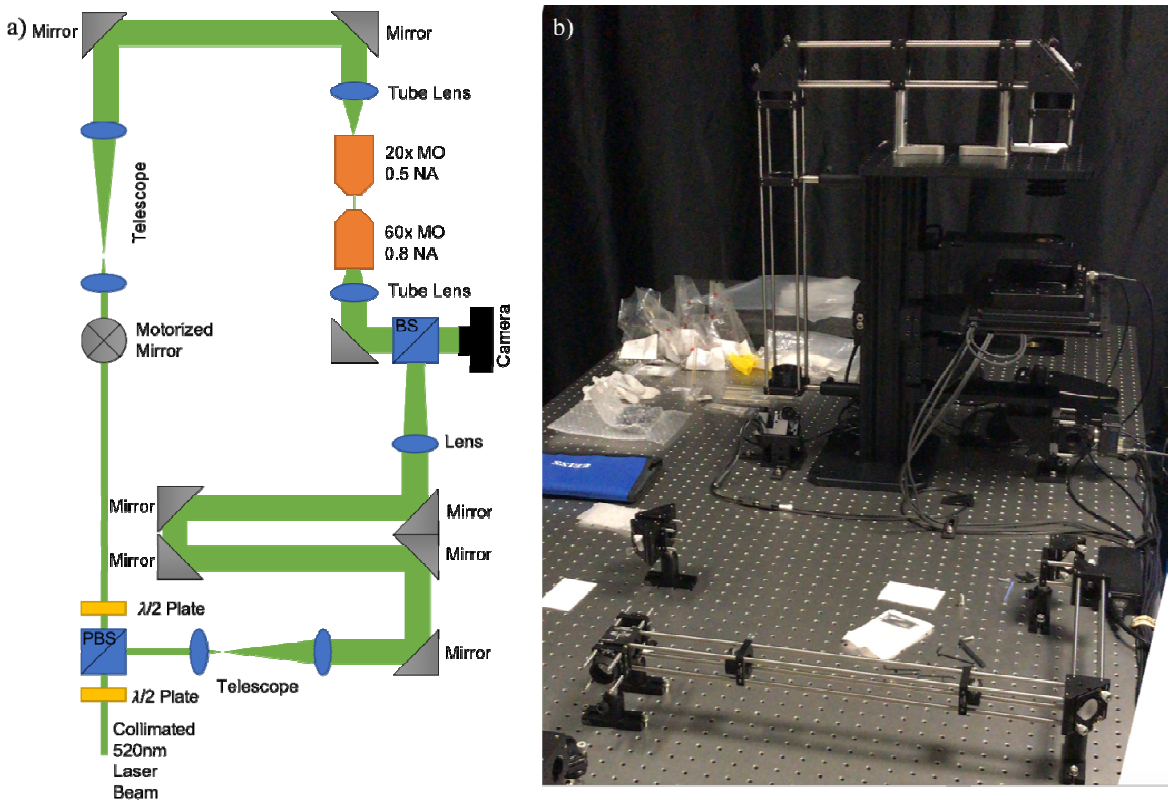

Figure 1. A simplified drawing (a) of the experimental setup and the photograph (b) of the actual setup

Holograms are acquired for different positions of the motorized mirror. For the illumination scan on a cone, approximately 100 holograms are acquired in total to be synthesized for tomographic reconstruction. The synthesis of holograms is implemented to form a volumetric stack of complex refractive index values [8].

3. RESULTS AND DISCUSSIONS

In the illumination angle scanning based tomographic approaches, range of the angular scan directly impacts axial resolution. For an optimal condition, angular scan half angle would be matched with the imaging objective NA. The axial resolution improves with the balanced increase of the half angle and NA. However, this increase poses a potential practical problem due to reduced working distances. In the configuration of the experimental setup, two opposed microscope objectives with both 0.5 NA are employed for scanning and imaging. Illumination angular scan is matched with the NA of the objective. The choice of the low NA enabled easily accessible working distance. However, the axial resolution is approximately 4um. In order to evaluate the imaging performance, a USAF 1951 test target is imaged using the setup. In figure 2, imaginary part of the complex refractive index is visualized for a volume stack. As expected, the axial resolution is poor in comparison to the lateral counterpart.

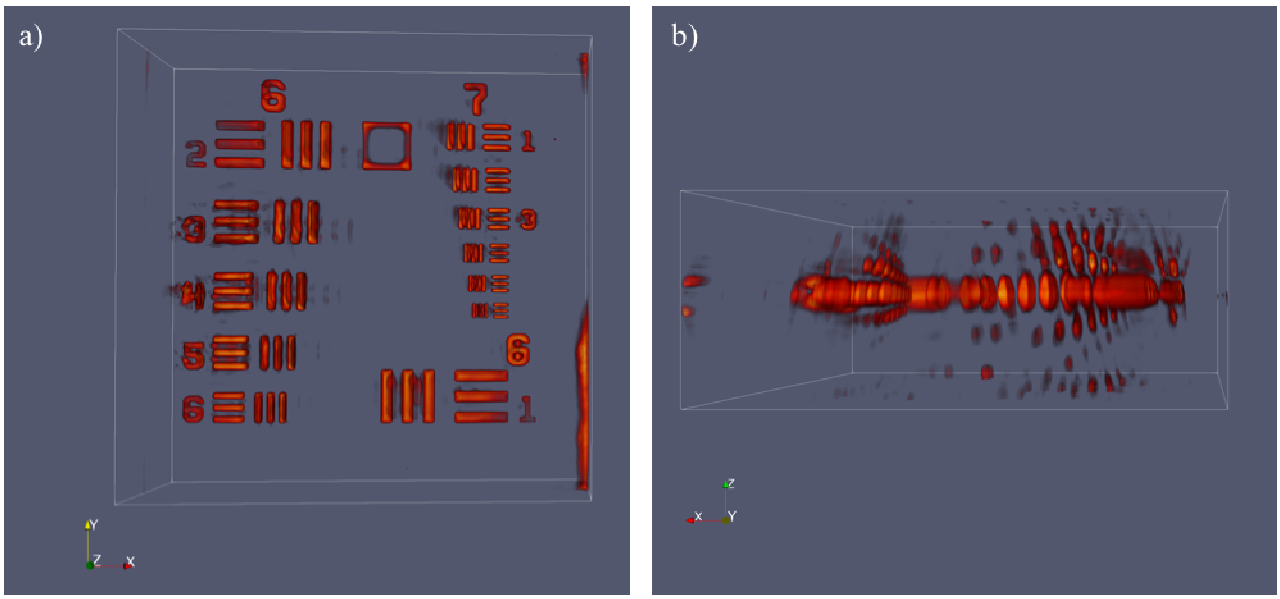

Figure 2. A volumetric reconstruction of USAF 1951 test target groups 6 and 7. Imaginary part of the complex refractive index is visualized in the negative form. Tangential (a) and axial (b) perspectives demonstrate the lateral and axial sectioning capability.

After the initial performance experiments, in vitro oligodendrocyte and neuron culture on 35mm glass bottom dish was imaged. Based on the cellular morphology, various field of views were chosen/ Central section of the real part of the refractive index for two different field of views are shown in figure 3. Figure 3 (a) shows a field of view without distinguishable myelin formation. The axons on the figure 3 (b) express an increase of refractive index on the outer edges that can be linked to increase of the angle between surface normal myelin structure and the incident light. The effective refractive index is expected to vary with the change of the incidence angle. In the case of myelinated axons, the surface normal to the axon changes from center to the edge due to the circular cross section. A region of interest marked with red dashed rectangle from figure 3 (b) is shown in figure 4 (a). This zoomed in region better illustrates the increase of the refractive index on the outer edges. Three dimensional variance filtered refractive index from this region emphasizes this change for better visualization. Orthogonal views of the variance filtered center sections from figure 4 (a) are shown in figure 4 (b) and (c). These orthogonal views demonstrate a large variance of refractive index on the outer edges where the myelination is expected to occur.

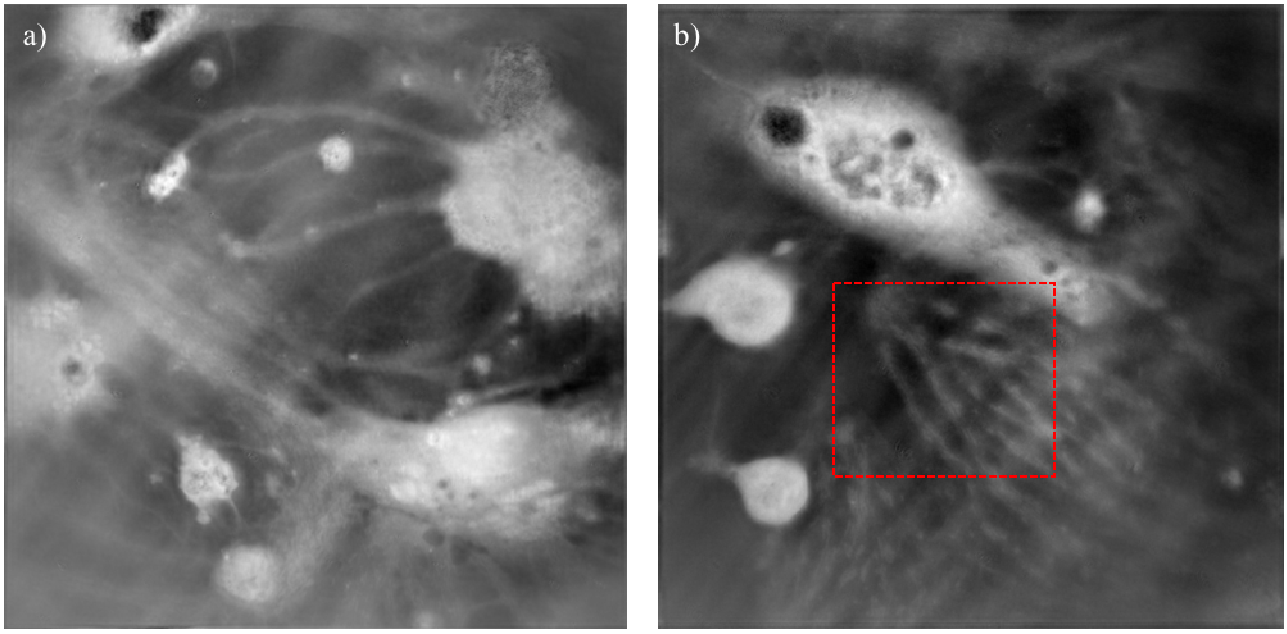

Figure 3. Center slice in axial direction from the real part of the refractive index field of views where not myelinated (a) and myelinated (b) axons are observable.

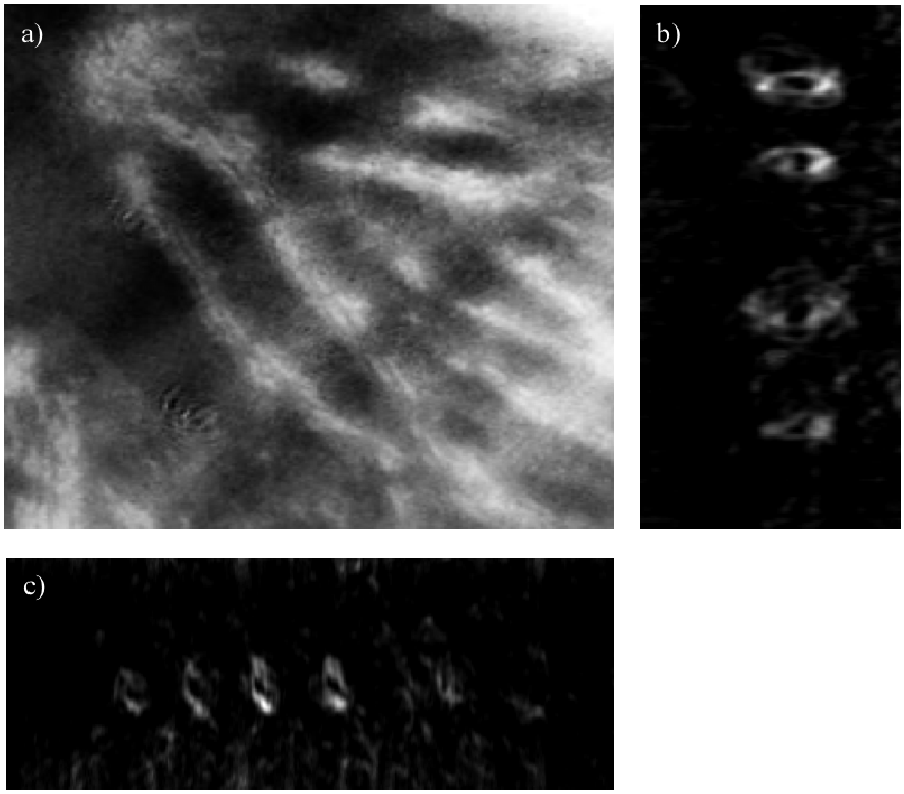

Figure 4. (a) Zoomed in and histogram stretched region from figure 3 (b) inside the red dashed rectangle. (b & c) Orthogonal views of 3D variance filtered version of figure 4 (a) from approximately center sections.

4. CONCLUSIONS

Myelination around axonal sections is challenging to image both in labeled and label free approaches. The alternating multiple layers of membrane, plasma, and medium forms a circularly symmetric periodic structure similar to Bragg fibers. The apparent refractive index is expected to change by the position of the incident light in the radial direction. This variation is exploited for label free imaging imaging of myelinating axons on a tomographic phase microscopy setup. The results show the increase of the refractive index on the outer edges of the myelinating axons and no apparent change for the non myelinated ones. Variance filtering in three dimensions further enhances the the outer edges where the myelination is expected.

ACKNOWLEDGEMENT

This work is supported by the Scientific and Technological Council of Turkey (TUBITAK) under grant No. 116F437. B. E. Kerman gratefully acknowledges the support of the Turkish Academy of Sciences.

REFERENCES

[1] Choi, W., Fang-Yen, C., Badizadegan, K., Oh, S., Lue, N., Dasari, R. R., & Feld, M. S. (2007). Tomographic phase microscopy. *Nature methods*, *4*(9), 717.
[2] Charrière, F., Marian, A., Montfort, F., Kuehn, J., Colomb, T., Cuche, E., ... & Depeursinge, C. (2006). Cell refractive index tomography by digital holographic microscopy. *Optics letters*, *31*(2), 178-180.
[3] Saab, A.S. and Nave, K.A. Curr Opin Neurobiol. 2017 Dec;47:104-112. doi: 10.1016/j.conb.2017.09.013
[4] Aydinli, F.I., Celik, E., Vatandaslar, B. K., and Kerman B. E., Myelin disorders and stem cells: as therapies and models, Turkish Journal of Biology, 40 (5), 1068-1080.
[5] Kwon, J., Kim, M., Park, H., Kang, B. M., Jo, Y., Kim, J. H., ... & Choi, M. (2017). Label-free nanoscale optical metrology on myelinated axons in vivo. *Nature communications*, *8*(1), 1832.
[6] Lim, H., Sharoukhov, D., Kassim, I., Zhang, Y., Salzer, J. L., & Melendez-Vasquez, C. V. (2014). Label-free imaging of Schwann cell myelination by third harmonic generation microscopy. *Proceedings of the National Academy of Sciences*, *111*(50), 18025-18030.
[7] Kerman, B. E., Kim, H. J., Padmanabhan, K., Mei, A., Georges, S., and Joens, M. S., Development, 142 (12), 2213-2225
[8] Cotte, Y., Toy, F., Jourdain, P., Pavillon, N., Boss, D., Magistretti, P., ... & Depeursinge, C. (2013). Marker-free phase nanoscopy. *Nature Photonics*, *7*(2), 113-117.